

Journal of Environmental & Earth Sciences

https://journals.bilpubgroup.com/index.php/jees

ARTICLE

Application of AFEP and RWP in Water Hazard Detection for Skip Mining Working Faces

Ping DU [®]

UCHN Energy Investment Group SHEN DONG COAL Geological Survey Company, Ordos 017000, China

ABSTRACT

In deep coal mining, skip mining techniques are increasingly adopted, yet their discontinuous extraction sequences and unique coal pillar support mechanisms create complex overburden failure patterns. This complexity gives rise to severe multi-source water hazards, including persistent threats from bed-separation water, goaf water accumulation, and structural water ingress. The intricate hydro-geological conditions, characterized by variable resistivity and significant electromagnetic interference, often render single geophysical detection methods inadequate, leading to interpretive ambiguities and potential oversight of critical risks. To address these challenges, this study innovatively proposes and demonstrates an integrated detection methodology that synergistically combines the Audio Frequency Electric Penetration (AFEP) method and the Radio Wave Penetration (RWP) method. The core innovation of this research is the design of a coordinated observation system meticulously tailored to the spatial distribution of coal pillars. Beyond data acquisition, a systematic, graded classification framework was established for the comprehensive analysis and fusion of the dual-method results. Crucially, these classification outcomes directly inform the formulation of targeted and tiered governance recommendations, translating detection data into actionable mitigation strategies. Practical application at the 22213 face yielded highly positive results. The integrated approach successfully delineated the spatial distribution of water-bearing anomalies and their connecting channels with a clarity unattainable by either method alone. This not only significantly enhanced the accuracy and reliability of the hydrological threat assessment but also provided a robust scientific foundation for implementing effective water hazard prevention and control measures, thereby ensuring the safe and efficient extraction of the skip mining face.

Keywords: Skip Mining Working Faces; Water Hazards; AFEP; RWP

*CORRESPONDING AUTHOR:

Ping DU, UCHN Energy Investment Group SHEN DONG COAL Geological Survey Company, Ordos 017000, China; Email: 7028829@qq.com

ARTICLE INFO

 $Received: 23\ June\ 2025\ |\ Revised: 4\ November\ 2025\ |\ Accepted: 14\ November\ 2025\ |\ Published\ Online: 1\ December\ 2025\ DOI: \ https://doi.org/10.30564/jees.v7i12.10606$

CITATION

DU Ping, 2025. Application of AFEP and RWP in Water Hazard Detection for Skip Mining Working Faces. Journal of Environmental & Earth Sciences. 7(12): 1–14. DOI: https://doi.org/10.30564/jees.v7i12.10606

COPYRIGHT

Copyright © 2025 by the author(s). Published by Bilingual Publishing Group. This is an open access article under the Creative Commons Attribution-NonCommercial 4.0 International (CC BY-NC 4.0) License (https://creativecommons.org/licenses/by-nc/4.0/).

1. Introduction

Coal mine water hazard accidents are characterized by their concealed nature, rapid onset, and severe consequences. In the event of a water inrush accident, minor cases may lead to increased drainage costs, elevated per-ton coal production costs, deterioration of the working environment, and tight mining succession schedules. Severe cases can result in casualties, flooding of mining areas or entire mines, difficulties in rescue operations, prolonged recovery periods, significant economic losses, and widespread social impacts [1–4].

Skip mining, as a specialized coal extraction method ^[5], involves reserving coal pillars at intervals to support the roof through staggered extraction, thereby reducing surface subsidence. This technique is particularly suitable for areas requiring special surface protection (e.g., under villages or infrastructure) and is also employed for mining across fault zones. However, the reserved coal pillars may amplify water hazard risks in skip mining areas, especially when crossing faults. Since faults inherently act as water-conducting channels, their hazard potential escalates during skip mining under water threat conditions. Therefore, pre-mining water hazard detection in target areas is crucial to enable timely mitigation measures.

Audio Frequency Electric Penetration (AFEP) and Radio Wave Penetration (RWP) are established geophysical techniques commonly employed for water hazard detection in underground coal mines [6]. However, these two methods exhibit fundamental differences in their detection principles and operational mechanisms. The AFEP method functions by injecting direct current into the formation and measuring the resulting voltage variations [7]. Its response primarily reflects changes in formation resistivity, demonstrating particular sensitivity to low-resistivity water-bearing anomalies. In contrast, the RWP method transmits low-frequency electromagnetic waves into the formation and detects variations in electromagnetic field strength [8]. Its response is mainly governed by electromagnetic wave attenuation characteristics, providing effective identification of water-conducting structures (such as faults and fractures) within high-resistivity formations.

The AFEP method is primarily utilized for detecting changes in formation water content $^{[9-12]}$, whereas RWP can not only identify water-bearing anomalies but also effectively characterize geological structural features $^{[13-17]}$. When a for-

mation contains water-rich zones without connected water-conducting structures, these areas generally do not pose immediate threats to mining operations. However, in skip mining faces, the combination of roof water accumulation and interconnected geological structures transforms the mining area into relatively vulnerable zones, posing significant threats to safe production^[18–20].

Consequently, reliance on a single method reveals substantial limitations under complex hydrogeological conditions: AFEP may fail to detect dry water-conducting structures, while RWP might underestimate isolated static water bodies unconnected to structural pathways. By integrating AFEP resistivity parameters with RWP attenuation parameters, synergistic detection of both "water sources" and "water-conducting channels" can be achieved. This integrated interpretation approach effectively overcomes the inherent ambiguities of single-method applications, significantly enhances spatial resolution and risk assessment accuracy, and provides more reliable technical support for water hazard prevention and control in skip mining faces.

This paper presents a case study of an actual skip mining face, detailing the scheme design and detection results of AFEP and RWP technologies in water hazard exploration. Analyze the detection differences between two detection methods in practical applications, comprehensively analyze the detection results of the two methods, and finally determine the water hazards that need to be paid attention to before mining. The study aims to provide technical guidance for water risk assessment and prevention in skip mining operations, particularly in geologically complex environments with fault zones.

2. Basic Detection Principles and Data Processing

2.1. AFEP Principle and Data Processing Method

The detection method of AFEP in coal mines is to establish a specific stable current field by laying power supply electrodes A (or A, B) in a tunnel of the coal mining face, and measuring electrodes M, N in an adjacent tunnel . Based on the potential difference of the measuring electrodes U_{MN} and the relative position relationship between the electrodes, the two electrical parameters of electric perspective are cal-

culated using Equation (1), and the occurrence state and influence range of geological anomalies in the exploration area are inferred based on this.

$$\begin{cases}
R = \frac{\Delta U_{MN}}{I} \\
\rho_s = K \frac{\Delta U_{MN}}{I}
\end{cases}$$
(1)

Where: ΔU_{MN} is the electrode potential difference measured, mV; I is the power supply current intensity, mA; K is the device coefficient of the electrical penetration method, R is the resistance, $\Omega \bullet$ m.

The specific detection process and data processing flow of the AFEP method in coal mines are as follows [21,22]:

- Data collection: Specific construction is carried out (1) in the tunnels on both sides of the working face to be detected. A transmitting electrode is arranged in one tunnel, and a receiving electrode is arranged in the other tunnel. The transmitting electrode group is energized to excite current, and the transmitting current is kept constant. The receiving electrode group receives potential difference data. When collecting data, it is necessary to determine the number of transmitting electrode groups, electrode spacing, and receiving electrode groups, electrode spacing, and other parameters based on the conditions of the tunnel site, in order to obtain sufficient effective data. The specific data collected is the voltage received by the receiving electrode.
- (2) Data pre-processing: The observation data collected from each electrode is organized in a certain format, usually stored in the form of a matrix or array, for subsequent processing and analysis. At the same time, preliminary filtering, denoising, and other processing can be performed on the data to remove some obvious outliers and interference signals. There are two types of interference that need to be removed in preprocessing: one is the power frequency interference in the tunnel, and the other is the metal support interference correction in the tunnel.
 - (a) The elimination of power frequency interference is achieved using the following formula:

$$H(z) = \frac{1 - 2\cos(2\pi T f_0)z^{-1} + z^{-2}}{1 - 2r\cos(2\pi T f_0)z^{-1} + r^2 z^{-2}}$$
 (2)

Where f_0 is the power frequency, T is the sampling interval, r is the bandwidth control factor (0.9 < r < 1).

(b) The following methods are used to correct the interference of metal support in the roadway:

$$E_{earth} = E_{total} - k \cdot B_{metal} \cdot \omega \qquad (3)$$

Where is the coupling coefficient, B_{metal} is the metal magnetic induction intensity, ω is the angular frequency.

- (3) Filtering processing: the filtering of AFEP data is generally processed using wavelet transform. By selecting appropriate wavelet functions and decomposition levels, the data is decomposed and reconstructed to achieve filtering of the signal.
- (4) Numerical imaging: discretize the underground space into multiple units, assuming that each unit has uniform electrical parameters, and obtain the electrical parameters of each unit by solving the corresponding equation, thereby achieving imaging of the underground geological body. According to the principle of electrical methods, the expression for the received potential difference vector is established:

$$\Delta U = X \cdot W \tag{4}$$

Where ΔU is the received potential difference vector, X is the matrix composed of the lengths r_j and i of the rays in each unit, and W is the electrical parameter vector of each unit.

As Equation (4) is an overdetermined system of equations, iterative methods are usually used to solve for its approximate solution, such as the Landweber iteration method:

$$W^{k+1} = W^k + \beta \cdot X^T \cdot (\Delta U - X \cdot W^k)$$
 (5)

where k is the number of iterations and β is the relaxation parameter.

After calculating the voltage distribution, calculate the distribution of resistivity based on the constant current emitted.

(5) Imaging interpretation: based on the distribution map of resistivity, analyze the low-resistance abnormal area. Generally, the low resistance area is the water containing an abnormal area, which is the area that needs attention during the production process. The conductivity is the reciprocal of resistivity. According to the AFEP detection results, if the conductivity is greater than the background value of the formation, it means that the resistivity is small and there may be a water hazard.

2.2. RWP Principle and Data Processing Method

The RWP detection method is to emit electromagnetic waves of a certain frequency into the formation. The propagation formula of electromagnetic waves in uniform space is as follows^[23–25]:

$$H = H_0 \frac{e^{-\beta r}}{r} \sin(\theta) \tag{6}$$

Where H_0 is a parameter determined by the transmission power of the instrument, r is the distance between the transmission point and the reception point, θ is the angle between the transmission and reception line and the vertical direction of the transmission borehole, and β is the electromagnetic wave absorption coefficient of the medium between the two points.

From Equation (6), it can be seen that the most signif-

icant factor affecting the size of the received signal is the absorption attenuation coefficient β of the rock, in addition to the transmission reception distance and spatial angle. The theoretical calculation formula for β is:

$$\beta = \omega \sqrt{\mu \varepsilon_r} \sqrt{\frac{1}{2} \left[\sqrt{1 + \left(\frac{\delta}{\omega \varepsilon_r}\right)^2} - 1 \right]}$$
 (7)

Where ω . μ , σ , and ϵ_r are the operating frequency of electromagnetic waves, rock permeability, rock conductivity, and dielectric constant, respectively. Therefore the most significant factor affecting signal strength in non-magnetic media with a fixed emission frequency is rock conductivity.

Due to the different electrical parameters of different formations(shown in **Table 1**), there are certain differences in the absorption of electromagnetic wave energy, especially in formations with lower resistivity, where the absorption effect of electromagnetic waves is more pronounced. The signals received by electromagnetic waves passing through the formation will vary. By analyzing the characteristics of the received radio waves, the distribution characteristics of the formation's resistivity can be analyzed through reverse engineering.

Table 1. Resistivity Values of Common Rock Types in Coal Measures.

Name	Mine Water	Shale	Coal	Sand	Limestone
Resistivity $(\Omega \cdot m)$	1 ~ 10	1 ~ 50	$10\sim10^4$	$1\sim10^5$	60 ~ 4×10 ⁵

In the actual detection process, electromagnetic waves are emitted on one side of the tunnel and electromagnetic wave signals are received on the other side. The specific process of inverting the electrical parameters of the medium based on the detection data is as follows:

 For the inversion of the electrical parameters of the medium in the test area, the electrical parameters of the medium can be discretized into a grid as shown in the Figure 1.

Calculate the length of each ray and its length in all grids, and rewrite Equation (6) as an integral along the path:

$$H_{\theta} = H_0 \frac{e^{-\int \beta(x,y)dr}}{R} \sin(\theta)$$
 (8)

Take logarithms on both sides and perform equivalent mathematical transformations:

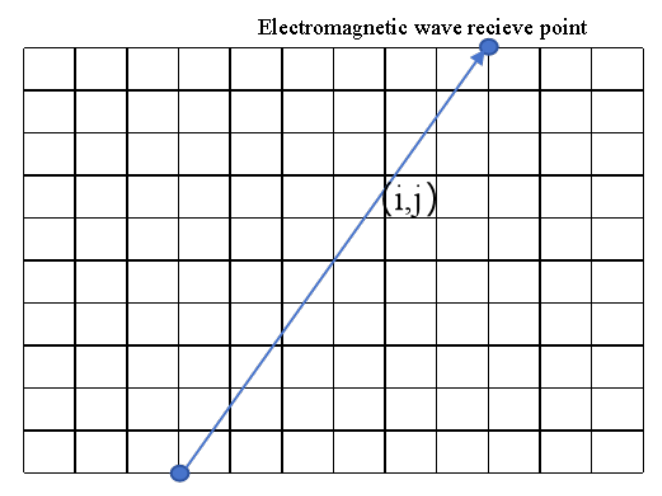
$$\ln \frac{H_{\theta}R}{H_0 sin(\theta)} = -\int \beta(x, y) dr \tag{9}$$

The integral of the absorption attenuation coefficient along the path is written in the form of a sum:

$$\sum_{j=1}^{n} \sum_{i=1}^{m} d(i,j)\beta(i,j) = p$$
 (10)

Write Equation (10) in the form of an equation:

$$D\beta^T = p \tag{11}$$



Electromagnetic wave emission point

Figure 1. The oblique relationship between a single ray and a grid.

Solve Equation (11) to obtain the distribution of absorption attenuation coefficients, and explain the distribution of electrical properties through the results of the solution Due to the pathological nature of the problem itself, multiple iterations are generally used to solve Equation (11). the preliminary iteration is as follows:

- (2) Given an initial solution x_0 , it can generally be set to 0.
- (3) Use the following formula for iteration:

$$x_j^i = x_j^{i-1} + \lambda \frac{p_i - \sum_{k=1}^N x_j^{i-1} A_{ik}^2}{\sum_{k=1}^N A_{ik}^2} A_{ij}$$
 (12)

Where is the value of the i-th iteration of the j-th grid, is the relaxation iteration factor between 0 and 2, is the projection value of the i-th ray, A_{ik} is the element value of the i-th row and k-column in the inversion matrix.

(4) Calculate the residual generated by the updated solution. If the residual meets the requirements for stopping the iteration, terminate the iteration process to obtain the final result. If it does not meet the requirements, return the new value to step 2 and iterate again until the final result is obtained.

3. Application

3.1. Geological Conditions

The rock strata in the mining field where the 22213 working face of a coal mine in Ordos is located are inclined

southwest at an angle of 1–3°, forming a gentle monocline structure. The eastern coal bearing strata are extremely gentle, with a dip angle of about 3 degrees towards the west. In the actual production process, the main geological structures are faults, and local areas expose erosion bodies. A normal fault (F11) with a drop of 15–25 m and a dip angle of 70° was discovered in the middle of the mine field. The fault direction is roughly consistent with the stratigraphic direction and extends for about 3600 m within the mine field.

During the mining process of the mine where the working face is located, a total of 11 faults were exposed, all of which are normal faults with small scales. Among them, 5 faults with a drop of less than 3 m, 1 fault with a drop between 3–5 m, 4 faults with a drop greater than or equal to 5 m, and 1 fault with a drop greater than 20 m were exposed.

The surrounding area of the working face excavation roadway is composed of unmined solid coal, and the surrounding rock is stable. The direct roof lithology of the coal seam is fine-grained sandstone, with a thickness of 8.88–13.26 m, an average of 9.15 m, and a compressive strength of 21.2–64.1 MPa; The direct bottom lithology is mudstone sandstone, with a thickness of 8.11–10.4 m, an average of 9.22m, and a compressive strength of 15.33–52.17 MPa; The main type of roof is Class II, with moderate hardness and moderate rockfall.

The thickness of the loose layer covering the working face is 20–75m, with an average of 70 m; the thickness of the bedrock covering the 12th coal seam is 70–95 m, with an average of 75 m. There is a fully mechanized mining area and

a goaf (refers to the void area remaining at the original ore body location after underground mineral resources (such as coal, metal ores, etc.) have been extracted.) in the upper part of the 12th coal seam. The distance between the 12th coal seam and the 22nd coal seam is 23–34 m, with an average of 30 m. The distance between the 12th coal seam and the 12th coal seam is 3–12 m, with an average of 10 m. There may be water accumulation in the low-lying points of the 12th coal seam, 12th coal roadway, and goaf in the upper part. There is no surface water body in the working face, and the main

water source for filling is the 12th coal and the goaf in 12th coal that have been fully mined and supplied by atmospheric precipitation leakage.

The 22213 working face is a skip mining working face with a total length of 1957 m, the 22213-1 working face is 489m long, the 2213-2 working face is 1274 m long, the skip mining area is 194 m long, and the working face is 272 m wide. The working face area that needs to be explored is the geophysical construction area marked in the schematic diagram in **Figure 2**.

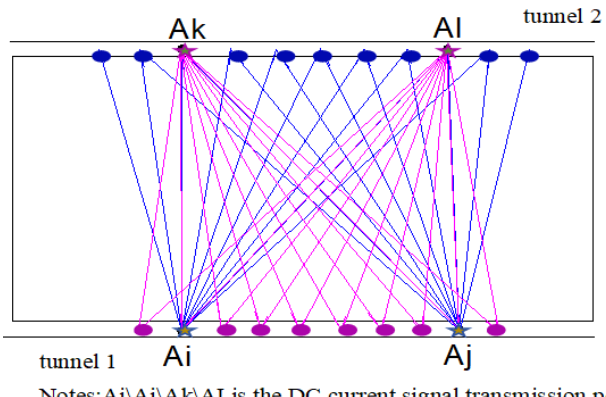


Figure 2. Schematic diagram of 22213 working face.

3.2. Construction Plan and Detection Results of AFEP

According to **Figure 1**, the 22213 working face is a skip mining working face, with a length of 489 m for the 22213-1 working face and a length of 1274m for the 2213-2 working face. The skip mining length is 194 m, and the working face width is 272 m. Therefore, detection is carried out in the two grooves of the coal mining working face, with one measuring point every 10 m and one power supply point every 50 m. For each power supply point, observe 1–21 points in the fan-shaped symmetrical interval of another trench to ensure that each unit in the mining area has two or more covers (as shown in **Figure 3**). For the 194 m area of skip mining, the main focus is to prevent changes in geological

stress caused by mining interference in the skip mining area. The key attention should be paid to the water content of the roof at the boundary of the skip mining area. Therefore, in the process of arranging measurement points, it is necessary to cover the boundary of the skip mining area, and arrange 3–5 measurement points to observe the boundary of the skip mining area. Therefore, the starting point of this audio electric penetration geophysical exploration project is the cutting eye of the working face, and the end point is the main retreat channel of the working face, with a total construction length of 1863 m. The transportation and return air ducts of the working face are both constructed, with 182 measurement points arranged in the transportation and return air ducts, 9 detection points in each lane, and a total of 373 measurement points in the two lanes.



Notes:Ai\Aj\Ak\AI is the DC current signal transmission point

- is the DC current signal recieve point for Ak\AI
- is the DC current signal recieve point for Ai\Aj

Figure 3. Audio Transmission Measurement Method.

The YT120 (A) AFEP (as shown in **Figure 4**) is used for this construction. The parameters of the instrument are list in **Table 1**. The instrument consists of two boxes: a power supply motor and a receiver. During operation, the power supply motor emits electrical signals into the formation at a certain frequency, while the receiver receives equal frequency signals in a certain area. The power supply voltage

is 300 V, the power supply current is 130 mA, the power supply time is 40 s, and the power supply frequency is f = 120 Hz. Single frequency point construction is carried out to explore the plane position, shape, and relative strength of water content in the water rich abnormal area of the top plate of the working face at a depth of 0–60 m. The main parameters is list in **Table 2**.



Figure 4. YT120 (A) AFEP instrument.

Table 2. The instrument parameters for YT120 (A).

Transmitter		Receiver		
Supply Voltage (V)	75, 150, 300	Measure voltage range (V)	0~2	
Power supply current (mA)	≤ 65	Current accuracy (%)	0.1 (@500 mV)	
Power supply frequency (Hz)	15, 30, 70, 120	Resolution (µV)	1	
Power supply time (s)	5, 10, 15, 20	Input impedance (M Ω)	10	
Current accuracy (%)	± 1	Weight (Kg)	7.5	
Weight (Kg)	9	2		

After collecting audio electrical transmission data from the 22213 skip mining face, consistency correction and tomographic inversion imaging analysis and processing were mainly performed on the audio electrical transmission data. The results of audio electrical transmission from the 22213 skip mining face are shown in **Figure 5**.

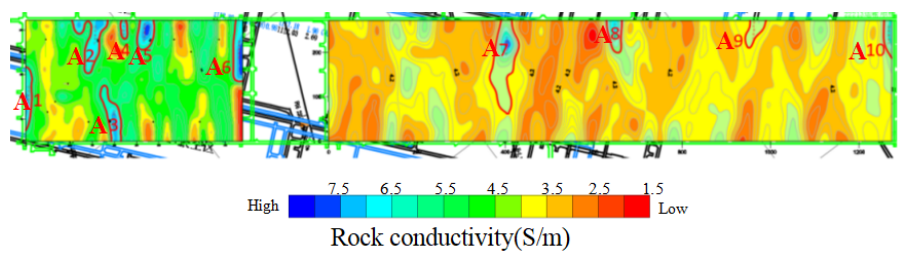


Figure 5. AFEP Results of 22213 skipping mining face.

According to **Figure 5**, the audio electric penetration results of the top plate 0–60 m of the skipping mining face mainly reflect the water rich situation of the overlying 12 coal goaf. The conductivity value of the rock layer in the 0–60 m section above the working face roof varies between 2.02–9.42 S/m, with an average value of 4.62 S/m and a standard deviation of 1.15 S/m.

The anomaly threshold of this rock layer section is

4.62 S/m which is the average conductivity of the roof strata. Based on the anomaly threshold of this rock layer, 10 anomalies were identified and named as A1, A2, A3,A4, A5,A6, A7, A8, A9, and A10, respectively. The anomalies are described as follows:

1) The No.1 abnormal area is located near the cutting line of the 22213-1 working face at a distance of 0–10 m,

- and the anomaly zone is irregularly distributed in a strip shape above the working face near the cutting eye side, with relatively strong amplitude.
- 2) The No. 2 abnormal area is around 102–184 m from the cutting eye of the 22213-1 working face, and the abnormal area is irregularly distributed in blocks above the working face near the 22213 transport channel side, with relatively strong amplitude.
- 3) The No. 3 abnormal area is around 167–215 m from the cutting eye of the 22213-1 working face, and the abnormal area is irregularly distributed in a strip shape above the working face near the 22214 transport channel side, with relatively strong amplitude.
- 4) The No.4 abnormal area is near the cutting line of the 22213-1 working face at a distance of 213–228 m, the abnormal area is irregularly distributed in a strip shape above the working face near the 22213 transport channel side, with relatively strong amplitude.
- 5) The No.5 anomaly is located at a distance of 257–290 m from the cutting eye of the 22213-1 working face. The anomaly area is irregularly distributed in blocks above the working face near the 22213 transport channel side, with relatively strong amplitude.
- 6) The No. 6 anomaly is located at a distance of 467–488 m from the cutting eye of the 22213-1 working face, at the edge of the skip mining area. The anomaly area is irregularly distributed in a strip shape above the working face near the main retreat channel of the 22213-1 transportation channel, with a relatively strong amplitude.
- 7) The No.7 anomaly is located near the cutting eye of 22213-2 working face at a distance of 364–429 m. The anomaly area is irregularly distributed in a strip shape above the working face near the transportation channel of 22213, with a relatively strong amplitude.
- 8) The No.8 abnormal area at the distance of 627–661 m from the cutting eye of the 22213-2 working face is irregularly distributed in blocks above the working face near the transportation channel side of 22213, with relatively strong amplitude.
- 9) The No.9 anomaly is located near the cutting eye of 22213-2 working face at a distance of 940–987 m. The anomaly area is irregularly distributed in blocks above the working face near the 22213 transport channel side,

- with a moderate amplitude.
- 10) The 10th anomaly is located near the cutting eye of 22213-2 working face at a distance of 1252–1270 m. The anomaly area is irregularly distributed in a strip shape above the working face near the main retreat channel of 22213-2 transportation channel, with relatively strong amplitude.

The positions of abnormal areas 1–6 are relatively concentrated above the 22213-1 working face, with a large range and relatively strong amplitude. By combining known geological data, the water content at the low-lying bottom of the 12 coal goaf overlying the working face is relatively high, with strong conductivity and amplitude.

3.3. Construction Plan and Detection Results of RWP

The detection method of radio wave perspective is the fixed-point method (as shown in Figure 6). The fixed-point method is that the transmitter is relatively fixed at a predetermined transmission point position in a roadway on the working face, and the receiver observes the field strength value point by point along the roadway within a certain range of adjacent roadways. The distance between the transmitting points is 50 m, and the distance between the receiving points is 10 m. For each transmitting point, observations are made at 6-11 points in the fan-shaped symmetrical interval of another trench to ensure that each unit in the mining area has two or more coverage. The construction of the pit penetration method roadway this time is carried out from the cutting of the working face to the direction of the retreat channel. Like the audio electric penetration construction, in order to ensure the safety of the skipping mining area, the boundary of the skipping mining area is covered during the layout of the measuring points. 3–5 measuring points are arranged on the boundary of the skipping mining area, with a total construction length of 1863 m. The geological structure distribution inside the working face is explored in the section.

The YDT-88 RWP instrument is used (as shown in Figure 7), the parameters of the instrument is shown in the Table 3. Considering the detection within the coal seam, the electrical characteristics of the coal seam, and the width of the working face, a radio wave penetration method at 880

kHz was selected for detection. After collecting RWP data from the 22213 skip mining face, the radio wave perspective data is mainly corrected, processed, tomographic imaging processed, and interpreted based on the transmission point position, reception point field strength value, etc. before data processing. The results of the radio wave perspective of the 22213 skip mining face are shown in **Figure 8**.

Figure 8 shows the distribution of the electric field

strength detected by the RWP method. Smaller field strength values indicate lower resistivity, which may suggest the presence of low-resistivity anomalous bodies, potentially corresponding to water-bearing channels. According to the radio wave perspective detection results in **Figure 8**, five obvious abnormal areas with strong relative attenuation were found, numbered as abnormal areas R1, R2, R3, R4, and R5 respectively.

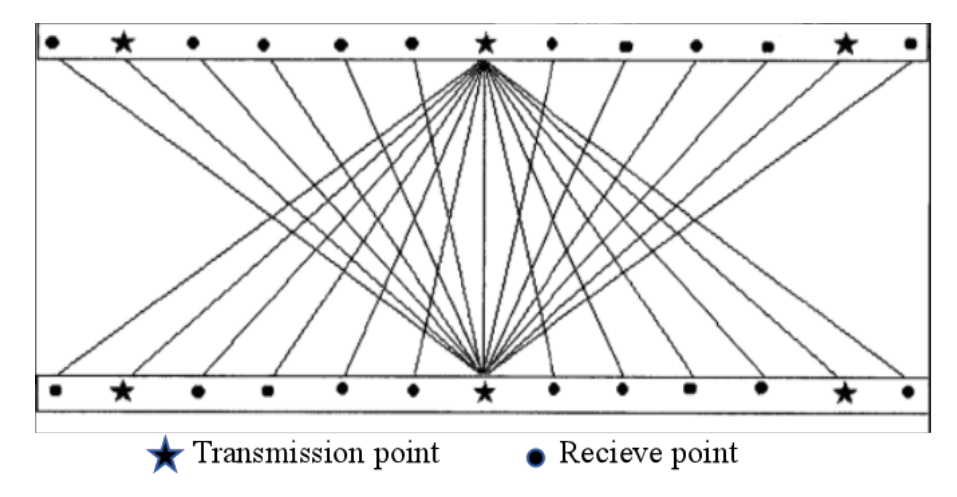


Figure 6. Schematic diagram of RWP fixed-point method transmission and reception range.



Figure 7. YDT-88 RWP instrument.

Table 3. The instrument parameters for YDT-88.

Parameter	Value
Operating Frequency (kHz)	365 ~ 965
Output Power (W)	1–2
Overall Bandwidth (Hz)	≥ 30
Receiving Sensitivity (mV)	≤ 0.06
Maximum Penetration Distance (m)	≥ 500
Continuous Operation Time (hours)	≥6

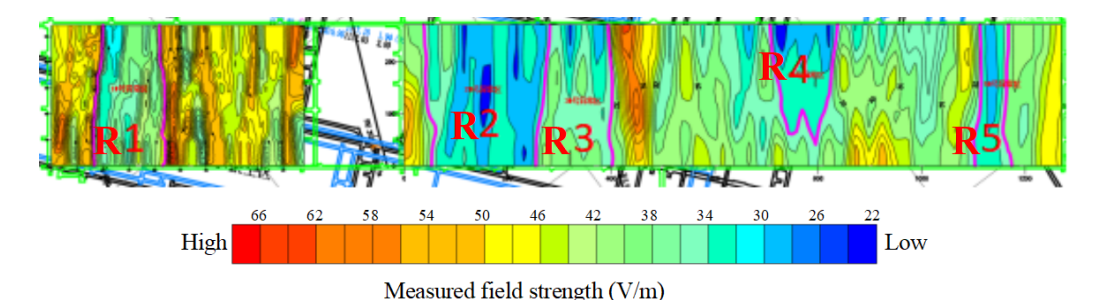


Figure 8. RWP Results of 22213 skipping mining face.

- The No.R1 abnormal area is distributed within the 22213-1 working face at a distance of 83–220 m from the cutting eye side, with a relatively strong amplitude. Combining the geological data revealed by the tunnel, it is possible that the attenuation anomaly zone is caused by faults, with an abnormal impact degree H > 1 coal thickness.
- 2) The No.R2 abnormal area is distributed within the 22213-2 working face, 40–280 m away from the cutting eye side, with relatively strong amplitude. Combining the geological data revealed by the tunnel, it is possible that the attenuation anomaly zone is caused by faults, with an abnormal impact degree of H < 1 coal thickness.
- 3) The No. R3 abnormal area is distributed within the 22213-2 working face, at a distance of 280–405 m from the cutting eye side, with a relatively strong amplitude. Combining the geological data revealed by the tunnel, it is possible that the attenuation anomaly zone is caused by faults, with an abnormal impact degree of H < 1 coal thickness.
- 4) The abnormal area No. R4 is distributed within the 22213-2 working face at a distance of 710–840 m from the cutting eye side, with relatively strong amplitude. It is speculated that the attenuation anomaly zone may be caused by faults or roadway undulations, with an abnormal impact degree of H < 1 coal thickness.
- 5) The abnormal area No. R5 is distributed inside the 22213-2 working face at a distance of 1102–1170 m from the cutting eye side, with relatively strong amplitude. Combining the geological data revealed by the tunnel, it is possible that the attenuation anomaly zone is caused by faults, with an abnormal impact degree of H < 1 coal thickness.

The amplitude of the 5 abnormal areas is relatively strong, the absorption coefficient is relatively high, and the measured field strength changes significantly. It is speculated that the abnormal areas may be geological anomalies caused by faults or roadway undulations.

3.4. Comprehensive Results

Based on the working principles of AFEP and RWP methods, AFEP primarily identifies water-bearing "Sources," while RWP detects water-conducting "Conduits" (structural pathways). The integration of both methods enables effective differentiation between mere water accumulation areas and critically dangerous water-transmitting pathways.

A critical step in our analysis was the spatial correlation between roof water-bearing anomalies (detected by AFEP) and in-seam structural anomalies (identified by RWP). Through systematic analysis, we have identified three distinct correlation patterns:

3.4.1. High-Risk Correlation: Direct Connection Between Conduits and Sources

Representative Zone: Structural anomaly R1 & water-bearing cluster [A2, A3, and A4].

Spatial Characteristics: R1 (83–220 m) shows near-perfect spatial overlap with A2 (102–184 m), A3 (167–215 m), and A4 (213–228 m), forming a continuous anomalous zone extending approximately 83–228 m from the cutting eye.

Parameter Corroboration: R1 displays strong amplitude response with an impact degree exceeding one coal seam thickness, indicating a significant fault; A2–A4 all show relatively strong responses with conductivity values reaching up to 9.42 S/m (over 200% of the background mean).

Risk Assessment: This zone presents the highest water

inrush risk. The R1 fault acts as a primary conduit, likely hydraulically connecting the water-saturated #12 coal goaf (represented by A2-A4 anomalies) directly to the active working face, creating high potential for sudden, concentrated water inrush.

3.4.2. Moderate-Risk Correlation: Potential or **Indirect Hydraulic Connection**

Representative Zone: Structural anomaly R2 & waterbearing anomaly A7.

Spatial Characteristics: R2 (40–280 m) and A7 (364–429 m) are adjacent but not directly overlapping, with A7 located at the distal end of the R2 anomaly trend.

Parameter Characteristics: R2 shows lesser impact degree (below one coal seam thickness), while A7 appears as an isolated water-bearing anomaly.

Risk Assessment: Suggests potential hydraulic connectivity where the R2 fault zone might influence or be influenced by the water-rich zone A7. The risk is moderate as the connection is less direct compared to the high-risk correlation.

3.4.3. Isolated Water-Bearing **Anomalies: Static Water Accumulation Risk**

Representative Anomalies: A1, A5, A6, A8, A9, and A10.

Characteristics: These anomalies represent water-rich zones in the roof with no RWP-detected structures directly beneath them.

Risk Assessment: Primarily indicates static water accumulation in goaf areas. While posing water hazards, the absence of major direct conduits suggests a lower probability of catastrophic inrush. However, roof collapse-induced water seepage remains a concern, requiring appropriate drainage measures.

3.4.4. Isolated Structural Anomalies: Geotechnical Stability Risk

Representative Anomalies: R3, R4, and R5.

Characteristics: These are structural anomalies (faults/fractures) with no overlying strong AFEP waterbearing anomalies.

Risk Assessment: These structures are likely nonwater-bearing or disconnected from main water sources. All show impact degrees below one coal seam thickness. Their primary risk relates to geotechnical hazards (ground control issues, roof stability problems) rather than immediate hydrological threats, though they should be monitored for potential future hydraulic connectivity.

This enhanced four-category classification system provides a more nuanced framework for risk assessment in skip mining operations, enabling targeted prevention strategies for each distinct hazard type. This systematic classification provides a practical framework for prioritizing water hazard mitigation measures in skip mining operations.

Based on the integrated analysis, the working face can be segmented into risk zones as shown in Table 4.

Table 4. The Risk classification results of detection results for working face 22213.

Risk Zone	Location (From Cutting Eye)	Anomaly Correlation	Interpretation & Risk
I: High	22213-1 Face, 83m-228 m	R1 + A2, A3, A4	Major water-conducting fault. High-potential for sudden water inrush. Requires immediate and pre-emptive action.
II: Moderate	22213-2 Face, 280–429 m	R2 (proximal to A7)	Potential fault-mediated water hazard. Risk of water inflow during mining.
III: Low (Static Water Accumulation Risk)	Various (e.g., A6, A8)	Isolated AFEP Anomalies	Static goaf water. Risk of seepage or localized drip water. Monitor during mining.
IV: Low (Geotechnical)	Various (e.g., R3, R4, R5)	Isolated RWP Anomalies	Dry faults. Primary risk is roof instability and caving.

conducting fault zone (R1)in the first 230 meters of the 22213-1 face, which is directly linked to overlying goaf water (A2-A4).

The most significant threat is a well-defined, water- to ensure the safety of coal mining in the skip mining face, we provide the following suggestions for reference by production personnel.

Priority Action in Zone I: Conduct targeted drilling Based on the comprehensive analysis results, in order into the R1&A2-A4 corridor for direct validation of water pressure and yield. Implement pre-conditioning measures such as grouting of the fault zone and/or pre-drainage boreholes from the gate roads towards the anomaly cluster.

Enhanced Monitoring in Zone II: Increase the frequency of microseismic monitoring and in-situ stress measurements as mining approaches the R2/A7 zone.

General Protocol: Maintain a strict protocol of "advance detection" (probe drilling) ahead of the face, especially when mining through all identified anomalous zones, regardless of their initial risk classification.

4. Conclusions

This study systematically investigates the issues of water hazard detection and prevention in skip mining faces. The skip mining method controls surface subsidence by leaving coal pillars and is suitable for special geological conditions, such as protected areas and fault zones. However, the retention of coal pillars alters the stress distribution in the surrounding rock, thereby exacerbating water hazard risks, particularly when combined with natural water-conducting channels (e.g., faults), posing significant safety hazards.

Based on the specific geological conditions of the 22213 skip mining face, this study designed and implemented a collaborative detection scheme integrating AFEP and RWP technologies. The AFEP survey identified 10 discrete anomalies, while the RWP survey detected five broader anomalous zones. Analysis confirmed the complementary advantages of the two methods: AFEP offers higher resolution for accurately identifying water-rich zones, whereas RWP provides broader coverage for detecting water-conducting structures. Based on the detection results, a four-tier risk classification system was established:

First, high-risk areas, characterized by overlapping AFEP and RWP anomalies, indicate the coexistence of water-bearing bodies and water-conducting channels, requiring thorough verification and treatment before mining. Second, moderate-risk areas, marked by adjacent anomalies, suggest potential hydraulic connections between water-bearing bodies and water-conducting channels, necessitating enhanced monitoring during mining. Third, isolated water hazard anomalies, detected only by AFEP, indicate static water accumulation without clear water-conducting channels, requiring vigilance against new water-conducting paths induced

by mining disturbances. Fourth, isolated structural anomalies, detected only by RWP, indicate the presence of water-conducting structures without current water filling, requiring attention to changes in surrounding hydrological dynamics.

The research results demonstrate that the integrated AFEP-RWP detection method significantly improves the accuracy and reliability of water hazard assessment in complex skip mining environments, providing a scientific basis for targeted prevention and control measures at the 22213 working face. Beyond this specific case, the integrated detection methodology and risk classification system established in this study offer a transferable technical framework for water hazard exploration and risk mitigation in similar complex mining conditions, directly contributing to mine safety and efficient extraction.

Funding

This work received no external funding.

Institutional Review Board Statement

Not applicable.

Informed Consent Statement

Not applicable.

Data Availability Statement

The data that support the findings of this study are derived from actual mine data, which cannot be made publicly available due to privacy and confidentiality restrictions. The data contain sensitive information about the mining operations and related parties that could potentially compromise the security and competitive position of the mining company involved. Access to such data is subject to strict regulations and agreements that prevent us from sharing the raw data outside of the research context.

Acknowledgments

I would like to express my sincere gratitude to *UCHN Energy Investment Group, SHEN DONG COAL Geological Survey Company* for their unwavering support throughout the duration of this research project. Their contributions have been instrumental in providing the necessary resources and environment that facilitated the successful completion of my work.

Conflicts of Interest

The authors declare no conflicts of interest.

References

- [1] Sun, W., Li, W., Ning, D., et al., 2023. The current situation, prediction and prevention suggestions of coal mine water accidents in China. Coalfield Geology and Exploration. 51(12), 185–194. (in Chinese)
- [2] Zeng, Y., Yu, C., Wu, Q., et al., 2023. Classification method of "three zones" for water prevention and control in coal mines and its significance in water hazard prevention and control. Journal of China Coal Society. 49(8), 3605–3618. DOI: http://dx.doi.org/10.13225/j. cnki.jccs.2023.0717 (in Chinese)
- [3] Dong, S., 2023. Application of Artificial Intelligence Technology in the Intelligent Development of Coal Mine Water Hazard Prevention and Control. Safety in Coal Mines. 54(5), 1–12. (in Chinese)
- [4] Zeng, Y., Wu, Q., Zhao, S., et al., 2023. Characteristics, causes, and prevention measures of coal mine water accidents in China. Coal Science and Technology. 51(7), 1–14. (in Chinese)
- [5] Dai, H., Yan, Y., Liu, C., et al., n.d. Coordinated full mining technology for thick coal seams and its practice in underground coal mining in villages. Journal of China Coal Society. 48(12), 4352–4364. (in Chinese)
- [6] Dong, J., 2006. Research on Visualization Methods for Electrical Exploration Data and Interpretation [Master's thesis]. Xi'an University of Science and Technology: Xi'an, China. (in Chinese)
- [7] Zeng, F., Wang, Y., Zhang, X., et al., 1997. Mine audio electric perspective and its application. Coalfield Geology and Exploration. 6, 54–57. (in Chinese)
- [8] Lu, J., Wang, Y., Cui, W., et al., 2023. Research on Physical Simulation Experiment of Monitoring Water Tank with Audio Electrical Perspective Method for Mine Water Hazards. Coal Science and Technology. 51(S1), 265–274. (in Chinese)
- [9] Xiao, Y., 2010. Study on radio wave penetration technology for mechanized coal face [Master's thesis]. Anhui University of Science and Technology: Anhui, China. (in Chinese)
- [10] Wu, Y., 2002. Research on Underground Electromagnetic Wave Detection and Application [PhD thesis]. Central South University: Changsha, Hunan. (in Chinese)

- [11] Zhang, P., Zhu, X., Sun, W., et al., 2022. Study on mechanism of delayed water inrush caused by mining-induced filling fault activation. Coal Science and Technology. 50(3), 136–143. (in Chinese)
- [12] Gao, Y., Gao, Y., Lu, Z., et al., 2022. Prevention and control technology of Ordovician water in Tangjiahui Coal Mine based on transparent geology. Coal Geology & Exploration. 50(1), 101–108. (in Chinese)
- [13] Liu, S., Fan, Z., Yin, X., et al., 2020. Key technologies for prevention and control of water-sand inrush disaster in fully mechanized caving mining under rich water aquifer. Journal of China Coal Society. 45(8), 2880–2889. (in Chinese)
- [14] Jin, D., Zhao, C., Duan, J., et al., 2020. Research on 3D monitoring and intelligent early warning system for water hazard of coal seam floor. Journal of China Coal Society. 45(6), 2256–2264. (in Chinese)
- [15] Liu, B., Li, S., Li, S., et al., 2010. Application of electrical resistivity tomography monitoring system to mine water inrush model test. Chinese Journal of Rock Mechanics and Engineering. 29(2), 297–307. (in Chinese)
- [16] Liu, B., Li, S., Nie, L., et al., 2012. Research on simulation of mine water inrush real-time monitoring of using electrical resistivity constrained inversion imaging method. Journal of China Coal Society. 37(10), 1722–1731. (in Chinese)
- [17] Zhao, X., Liu, S., Li, F., et al., 2008. Study on resistivity abnormal characteristics of coal seam floor failure. Chinese Journal of Engineering Geophysics. 2, 164–168. (in Chinese)
- [18] Lu, J., 2016. 3D electrical resistivity inversion and imaging technology for coal mine water-containing/water-conductive structures. Journal of China Coal Society. 41(3), 687–695. (in Chinese)
- [19] Lu, J., 2016. Simulation study on electrical penetration anomalous features of hidden water-bearing fault in working face. Coal Science and Technology. 44(8), 168–175. (in Chinese)
- [20] Zhang, J., Zhang, T., Wang, X., et al., 2020. Research on correction method of audio frequency electric perspective detection for low resistivity body in surrounding rock of roadway. Coal Science and Technology. 48(11), 182–190. (in Chinese)
- [21] Cao, S., Dong, F., Cheng, W., et al., 2022. Study on the development height of "two zones" of coal seam roof based on parallel electric method. Mining Safety & Environmental Protection. 49(3), 94–100. (in Chinese)
- [22] Lu, J., Wang, B., Li, D., et al., 2022. Application of mine-used resistivity monitoring system in working face water disaster control. Coal Geology & Exploration. 50(1), 36–44. (in Chinese)
- [23] Pidlisecky, A., Haber, E., Knight, R., 2007. RESINVM3D: A 3D resistivity inversion package. Geophysics. 72(2), H1–H10. DOI: https://doi.org/10.

1190/1.2402499

[24] Liu, S., Liu, X., Jiang, Z., et al., 2008. Research on electrical prediction for evaluating water conducting fracture zones in coal seam floor. Chinese Journal of Rock Mechanics and Engineering. 28(2), 348–356.

(in Chinese)

[25] State Administration of Coal Mine Safety, 2018. Detailed rules for water prevention and control in coal mines. Coal Industry Press: Beijing, China. (in Chinese)